Volume 15, Number 2, 2022. pp. 107-118

Jordan Journal of Physics

ARTICLE

Ab-initio and Monte Carlo Simulations of the New Half-Heusler Alloy NiCrGa

S. Idrissi[a], **H. Labrim**[b,c], **S. Ziti**[d] and **L. Bahmad**[a]

[a] *Laboratoire de la Matière Condensée et des Sciences Interdisciplinaires (LaMCScI), Mohammed V University of Rabat, Faculty of Sciences, B.P. 1014 Rabat, Morocco.*

[b] *USM/DERS/Centre National de l'Energie, des Sciences et des Techniques Nucléaires (CNESTEN), Rabat, Morocco.*

[c] *Advanced Systems Engineering Laboratory, National School of Applied Sciences, Ibn Tofail University, Kénitra, Morocco.*

[d] *Intelligence Artificial and Security of Systems, Mohammed V University of Rabat, Faculty of Sciences, B.P. 1014 Rabat, Morocco.*

Doi: **https://doi.org/10.47011/15.2.1**

Received on: 20/08/2020; *Accepted on: 6/12/2020*

Abstract: In this work, we are investigating the electronic and magnetic properties of the new NiCrGa half-Heusler alloy (HHA), by using the *ab-initio* and Monte Carlo simulations (MCSs). The *ab-initio* method is performed under the pseudo-potential method and the generalized gradient approximation GGA. The density of states (DOS) and the band structure calculations show that the alloy NiCrGa reveals a nearly half-metallic (HM) behavior. In particular, the Slater-Pauling (SP) rule has been confirmed when using the magnetic moments of the individual constituents of the NiCrGa compound. The Monte Carlo simulations (MCSs) are accomplished using the Metropolis algorithm. In order to determine the transition temperature, we are based on the behavior of the total magnetization and susceptibility of this material. We also presented and discussed the hysteresis loops of the half-Heusler compound, for fixed values of temperature, exchange coupling interactions and crystal field. It is found that when increasing the crystal field, the surface of the loops increases and *vice versa*.

Keywords: Half-Heusler alloy, NiCrGa, Slater pauling, DFT method, Monte Carlo study.

1. Introduction

The recent development of spintronics has attracted much attention by several researches [1-4]. The common character of materials used in the spintronic applications is the half-metallic ferromagnets behavior [5-10]. The first materials expected to be half-metallic ferromagnets were the half-Heusler alloys NiMnSb and PtMnSb. These alloys crystallize in cubic $C1_b$ structure [11–15]. In addition, the Heusler alloy NiMnSb has been described to exhibit a high Curie temperature [16]. It also possesses an integral magnetic moment of 4.00 μ_B per unit cell [17–21]. The Heusler alloys fall into three separate categories: half-Heusler, full Heusler and equiatomic quaternary Heusler with XYZ, X2YZ and XYMZ formulations, respectively, where X, Y and M are usually atoms of transition metals or alkali-earth metals and Z is a main group element.

Recently, a number of half-Heusler alloys have been studied, such as: NaZrM (M =P, As, Sb) [22], LiMnZ (Z=N, P, Si) [23], XYZ (X =Li, Na, K and Rb, Y=Mg, Ca, Sr and Ba, Z=B, Al and Ga) [24], MnPK [25] and LiZnM (M =P and As) [26]. On the other hand, the half-Heusler alloys have shown promising half-metallic behaviors. For example, the half-

Corresponding Author: S. Idrissi **Email**: samiraidrissi2013@gmail.com

Heusler alloy LiCrS shows a half-metallic property at its parameter of optimized lattice constant with the magnetic moment value of 5.00 μ_B [22, 27]. Moreover, Luo *et al*. [28] have performed the electronic and magnetic properties of the half-Heusler alloys: NiCrAl, NiCrGa and NiCrIn using the density functional theory (DFT). There are some other computational research studies on the other half-Heusler materials [29-31]. In addition, several Ni-based half-Heusler alloys have been investigated, such as: NiCrZ (Z = Si, Ge, Ga, Al, In and As) [32] and NiCrGa [33].

The purpose of this paper is to combine the *ab-initio* and Monte Carlo simulations to investigate the half-metallic behavior and the critical magnetic properties of the Ni-based half-Heusler alloy NiCrGa. We present our results in the framework of the *ab-initio* study, using the density functional theory (DFT) method under the Quantum Espresso package. On the other hand, we perform the Monte Carlo simulations under using Metropolis algorithm. Indeed, some of our recent works have been based on such simulations applying not only the DFT method, but also other numerical simulations [34, 35].

This work is organized as follows: In Section 2, we present and discuss the first principles and calculations. In Section 3, we illustrate the obtained results of *ab-initio* method including the density of states and band structures of the half-Heusler alloy NiCrGa. Also, the Slater Pauling rule is presented and discussed. In Section 3, we present the method and the computational procedures of the Monte Carlo simulations. Finally, we discuss the obtained results of the latter method in Section 4 and we give a summary in Section 5.

2. The *Ab-initio* Method for the NiCrGa Half-Heusler Alloy

2.1 Structural Properties

The first principles and calculations were performed using the Quantum Espresso (QE) package [36], combined with the Density Functional Theory (DFT), in order to investigate the electronic and magnetic properties of the half-Heusler alloy NiCrGa. For this purpose, we have applied the ultra-soft pseudo-potential approximation [37]. This method was used to calculate the interaction between the atom core and valence electrons in the studied alloy. Furthermore, the exchange and correction between electrons were calculated by the generalized gradient approximation (GGA) [38-39]. In the Brillouin zone integrations, we take 5x5x5 k-points. The plane-wave basis is set to a cut-off energy value of 25 Ry. The convergence energy is taken to be 10^{-6} eV/atom.

The NiCrGa half-Heusler alloy (HHA) crystallizes in the cubic structure belonging to the space-group F-43m (216), as can be seen in Fig.1. Our simulation has been performed choosing the experimental lattice parameter value a = b = c = 5.80 Å [33]. The NiCrGa alloy (XYZ) crystallizes in the $C1_b$ structure, with Ni (X), Cr (Y) and Ga (Z) atoms occupying the Wyckoff positions: 4c (1/4, 1/4, 1/4), 4b (1/2, 1/2, 1/2) and 4a (0, 0, 0), respectively. These positions are derived from Ref. [33]. On the other hand, the VESTA package [40] was used to illustrate the geometry of the studied alloy, see Fig.1.

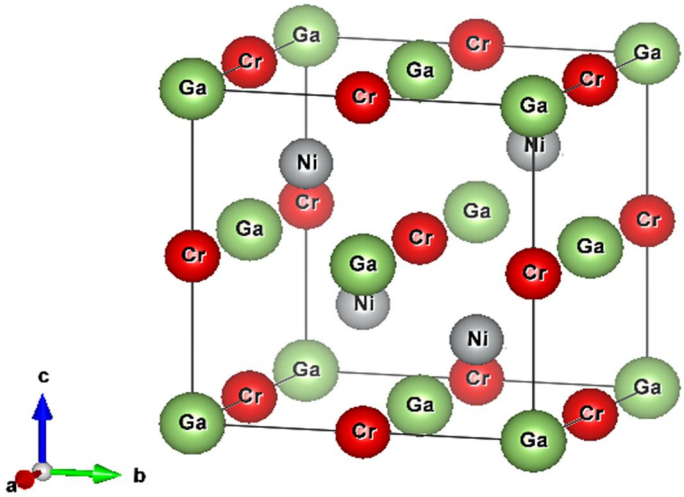

FIG. 1. The geometry of the half-Heusler alloy NiCrGa, using VESTA software [40].

2.2 Results of the *Ab-initio* Method

In order to investigate the total and the partial density of states (DOS) of the half-Heusler alloy NiCrGa, we report our results in Figs. 2(a) and 2(b), respectively. In fact, Fig. 2(a) represents the total density of states for spin-up and spin-down of the NiCrGa alloy. The non-symmetry between spin-up and spin-down states confirms the magnetic behavior of the studied material. Also, at Fermi level, there are states of spin-up, while there is almost an absence of spin-down states. Such behavior supports the nearly HF character of this compound. This finding is in good agreement with [32-33]. On the other hand, the partial density of states of the half-Heusler alloy NiCrGa for the individual elements: Ni, Cr and Ga is presented in Fig. 2(b). From this figure, it is found that the Cr and Ni elements are the most contributing to the total DOS of the NiCrGa compound, while, the Cr element is the only element contributing to the conduction band (CB). Moreover, the magnetic behavior of the half-Heusler alloy NiCrGa comes mainly from the transition metals: Ni and Cr.

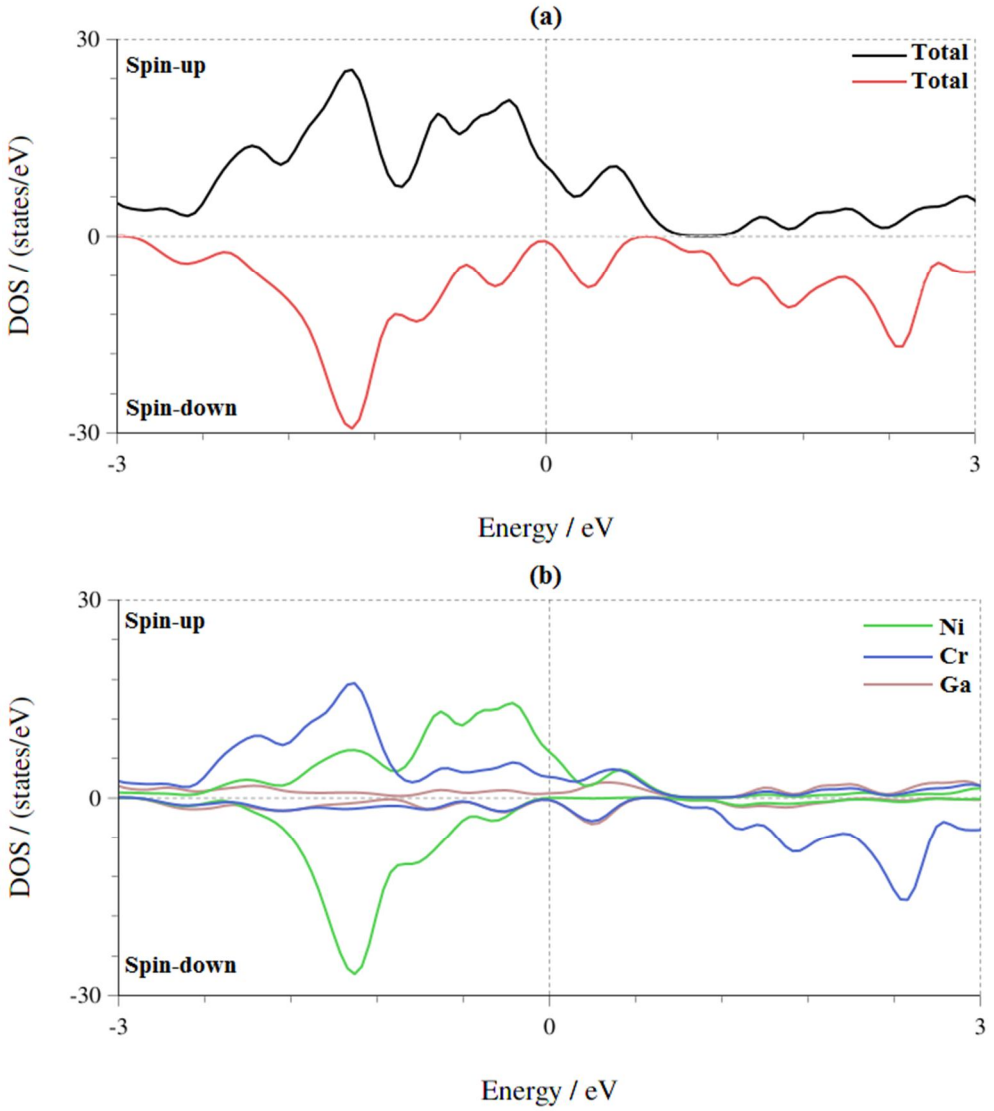

FIG. 2. Total (a) and partial (b) density of states of the half Heusler alloy NiCrGa.

To investigate the band structures of the half-Heusler alloy NiCrGa, we plot in Figs. 3(a) and 3(b) the obtained results for spin-up and spin-down states, respectively. From these figures, it is clear that at Fermi level, there are states of spin-up in Fig. 3(a), while there is almost an absence of spin-down states, see Fig. 3(b). In other words, the studied material gathers two behaviors: a metallic one in the spin-up channel and a near semi-conductor one in the spin-down channel. In this latter situation, the band gap value in the spin-down channel is almost equal to 0.4 eV.

When combining the results of density of states, see Figs. 2(a) and 2(b), and those of the band structures, see Figs. 3(a) and 3(b), we conclude that the NiCrGa alloy exhibits a nearly HM behavior.

Concerning the (SP) rule, it can be defined in this study following Refs. [41-43] that:

$$M_T = N_v\text{-}18 \quad (1)$$

M_T: Total spin magnetic moment.

N_v: Total number of valence electrons.

To explicit the valence electrons for the Heusler alloy NiCrGa unit cell, we use the electronic configurations for individual atoms: $4s^2 3d^8$ for Ni, $4s^1 3d^5$ for Cr and $4s^2 4p^1$ for Ga. Hence, the total number of valence electrons (N_v) of the Heusler alloy NiCrGa is close to 19. Using Eq. (1) of the Pauling Slater rule, we found that $M_T = 1.00\ \mu_B$. This result is confirmed in Table 1 for the total and the partial magnetic moments of the (HHA) NiCrGa. This table summarizes the total and partial magnetic moments of the (HHA) NiCrGa with the individual magnetic moment value of each element: m(Ni), m(Cr) and m(Ga).

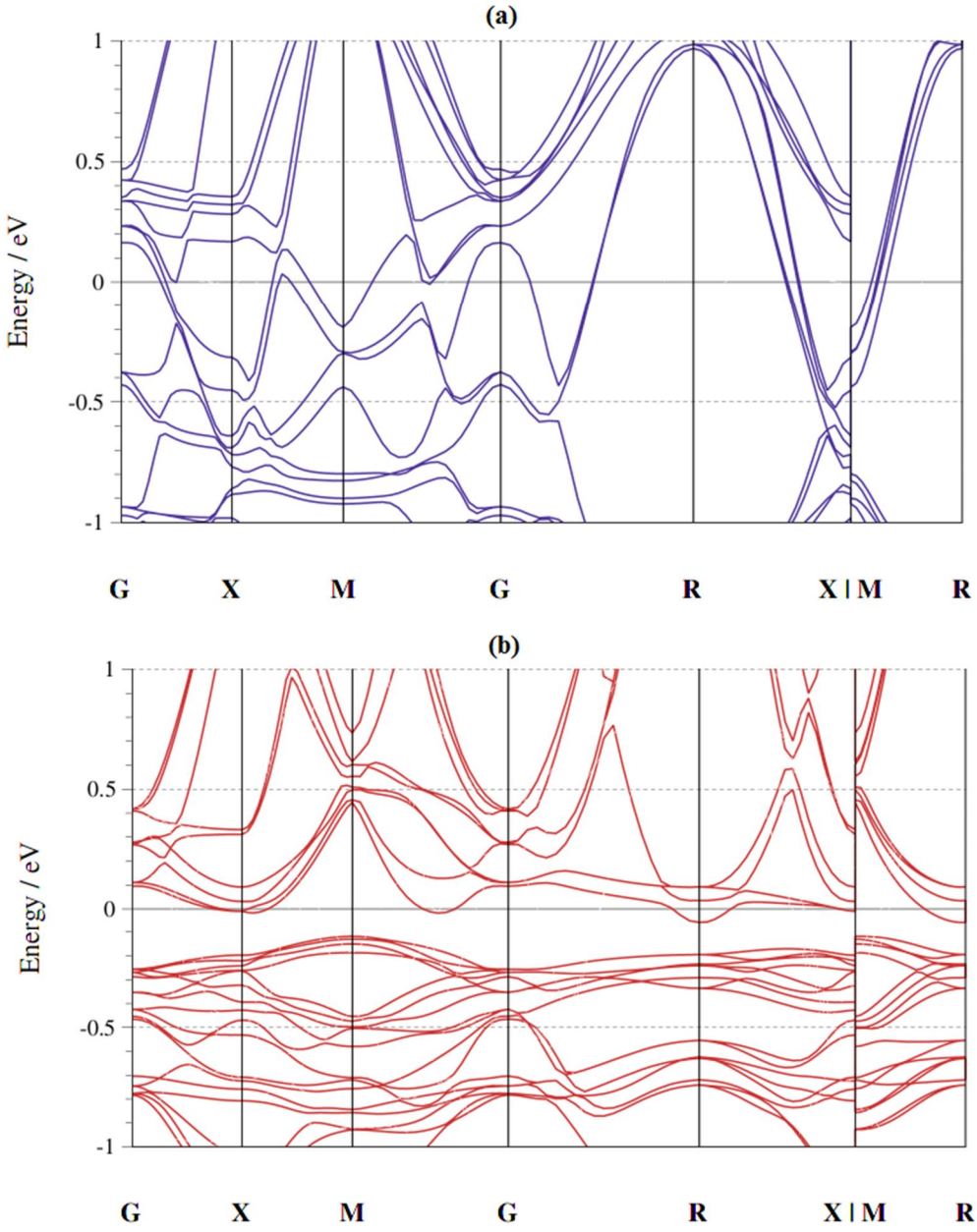

FIG. 3. Band structures of the half-Heusler alloy NiCrGa: (a) spin-up and (b) spin-down.

TABLE 1. Total and partial magnetic moments of the half-Heusler alloy NiCrGa with individual magnetic moment value of each element: m(Ni), m(Cr) and m(Ga).

Half-Heusler alloy	*m(Ni)* (μ_B)	*m(Cr)* (μ_B)	*m(Ga)* (μ_B)	M_{Total}(μ_B)	Slater Pauling rule M_T (μ_B)
NiCrGa	0.51	1.60	-0.44	1.67	1.00

3. Powder X-Ray Diffraction Patterns of the NiCrGa Heusler alloy

To simulate the powder X-Ray diffraction patterns (diffractograms) of the NiCrGa Heusler alloy in the $C1_b$ structure, we use the VESTA software package [40]. The powder X-Ray diffraction patterns (diffractograms) of the studied Heusler alloy are presented in Fig. 4. It is found that the theoretical XRD spectrum is similar to the experimental one shown in Ref. [33]. Indeed, a more intense peak is appearing at the (220) plane. Such behavior is a specific character of single crystals.

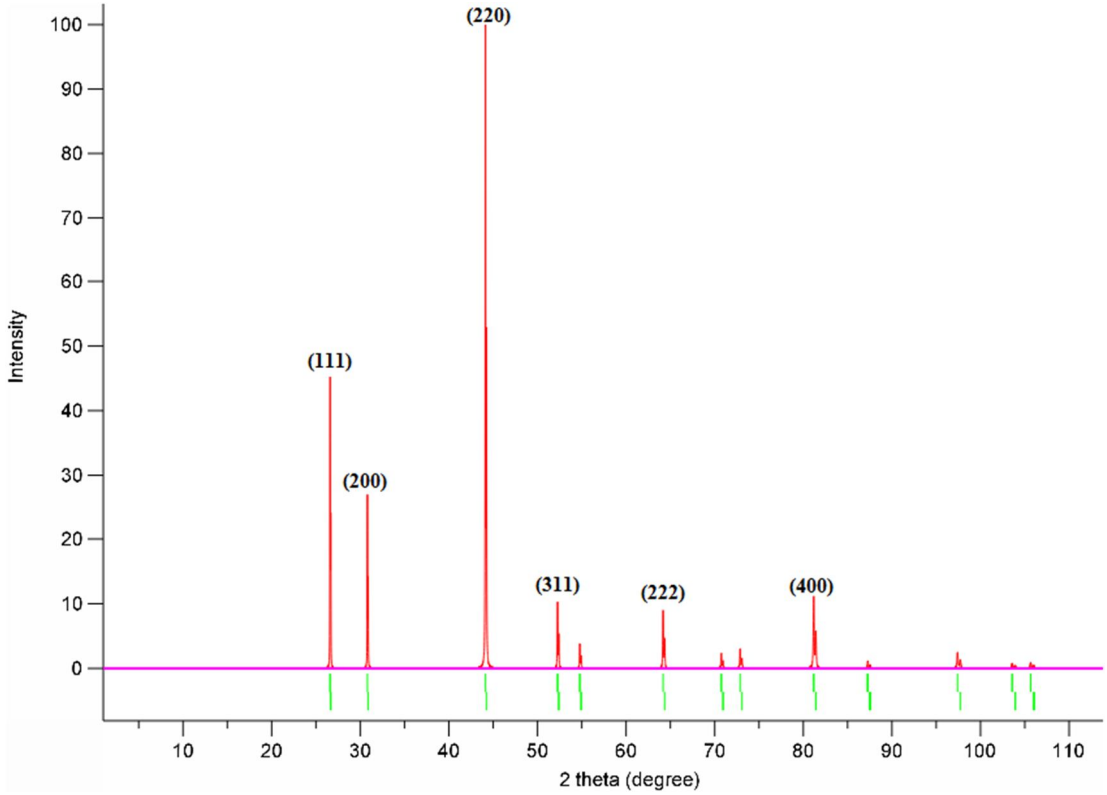

FIG. 4. Powder X-Ray diffraction patterns of Heusler alloy NiCrGa using the Vesta software.

4. Method of Monte Carlo Simulations

4.1 Methodology of Simulations

Since the studied compound contains the magnetic elements Ni and Cr as highlighted in Section 2 by the *ab-initio* method, we apply the MCS in order to deduce the critical magnetic behavior of the NiCrGa alloy. Hence, we propose the Hamiltonian of Eq. (2) to study the magnetic properties of the half-Heusler compound NiCrGa. The calculations are accomplished under the Metropolis algorithm. The periodic boundary conditions are imposed to the unit cell lattice. The results of the studied system are obtained for the specific super-cell size 5x5x5. For each spin configuration, we implement 10^5 Monte Carlo steps. For each MCS, all sites of the system are visited individually. A single-spin flip attempt is accepted or rejected according to the Boltzmann statistics.

The Hamiltonian modeling the half-Heusler alloy NiCrGa can be expressed as:

$$\left.\begin{aligned}\mathcal{H} = &-J_{Ni-Ni}\sum_{i,j} S_i S_j \; -J_{Cr-Cr}\sum_{k,l}\sigma_k\sigma_l \\ &-J_{Ni-Cr}\sum_{i,k} S_i\sigma_k \; - H\sum_i (S_i+\sigma_i) \\ &-\Delta_S\sum_i S_i^2 - \Delta_\sigma\sum_i \sigma_i^2\end{aligned}\right\} \quad (2)$$

where the magnetic spins S_i = 1 correspond to the Ni atoms, while σ_i=2 represents the Cr atoms.

The exchange coupling interactions are: $J_{Ni\text{-}Ni}$ between Ni atoms, $J_{Cr\text{-}Cr}$ between Cr atoms and $J_{Ni\text{-}Cr}$ between Ni- Cr atoms.

It is worth to note that the exchange coupling is the way in which two magnetic atoms (or ions) in a specific material interact with each other. When two magnetic atoms are situated very close together, their electrons can interact directly, in the same way as when forming a chemical bond.

For simplicity, we will limit this study to the unique crystal field: $\Delta = \Delta_S = \Delta_\sigma$, where Δ_S is the crystal field of the Ni ions and Δ_σ is the crystal field of the Cr ions.

The total energy per site is given by:

$$E_T = \frac{1}{N} < \mathcal{H} > \quad (3)$$

where N= N_σ + N_S, with N_σ and N_S being the numbers of σ- and S-atoms in the super cell unit, respectively.

The partial and total magnetizations are expressed as:

$$m_S = \frac{1}{N_S}\sum_i S_i \quad (4)$$

$$m_\sigma = \frac{1}{N_\sigma}\sum_i \sigma_i \quad (5)$$

$$m_T = \frac{N_\sigma m_\sigma + N_S m_S}{N_\sigma + N_S} \quad (6)$$

The partial and total susceptibilities are given by:

$$\chi_S = \frac{<M_S{}^2> - <M_S>^2}{K_B T} \quad (7)$$

$$\chi_\sigma = \frac{<M_\sigma{}^2> - <M_\sigma>^2}{K_B T} \quad (8)$$

$$\chi = \frac{<M_T{}^2> - <M_T>^2}{k_B T} \quad (9)$$

where $\beta = \frac{1}{k_B T}$ and k_B is the Boltzmann constant. T is the absolute temperature. In the following part, we will assume that k_B=1.

4.2 Results of Monte Carlo Simulations

The obtained results of the MCS concerning the thermal behavior of the partial and total magnetizations and susceptibilities of the HHA NiCrGa atoms are plotted in Figs. 5(a), 5(b) and 5(c) for H=1, Δ=1 and $J_{Ni\text{-}Ni}$= $J_{Cr\text{-}Cr}$=$J_{Ni\text{-}Cr}$= 1. In fact, Fig. 5(a) represents the magnetization and susceptibility of the individual Ni atoms. From this figure, it is clear that for very low temperature values, the magnetization undergoes the value m_S =1. Moreover, the peak of the susceptibility corresponds to the critical temperature value Tc ≈ 20 K. Concerning the individual magnetization and susceptibility of the Cr atoms, the obtained results are summarized in Fig. 5(b). This figure confirms the value m_σ = 2 for very low temperature. Also, the peak susceptibility is located at Tc≈20 K. The total magnetization and susceptibility of the (HHA) NiCrGa are presented in Fig. 5(c). From this figure, it is found that for low temperature values, the results of the ground state phase of the total magnetization show that m_T = (m_S+m_σ)/2 = 1.5.

Fig.5 (a)

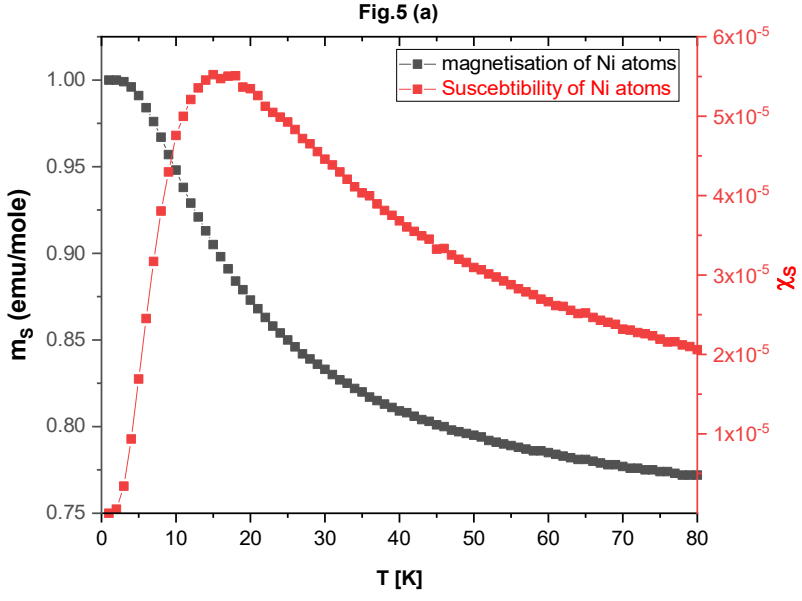

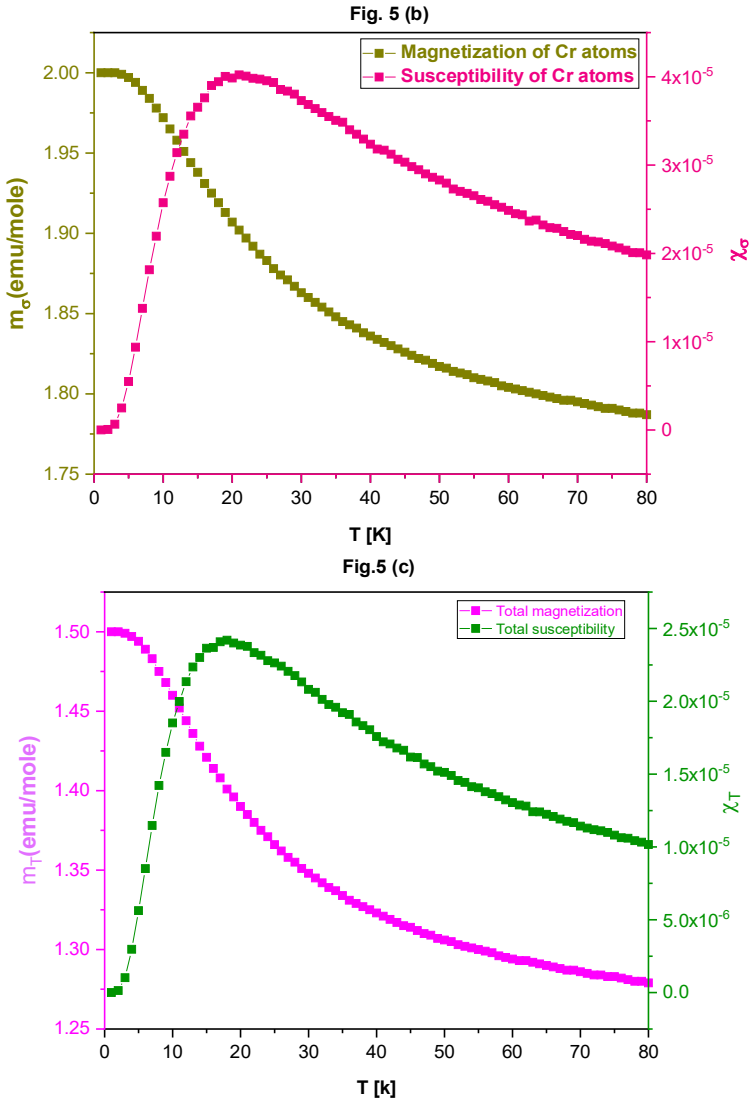

FIG. 5. The thermal behavior of the half-Heusler alloy NiCrGa for H = 1, Δ = 1 and $J_{Ni\text{-}Cr} = J_{Cr\text{-}Cr} = J_{Ni\text{-}Ni} = 1$: (a) the partial magnetization and susceptibility of Ni atoms, (b) the partial magnetization and susceptibility of Cr atoms and (c) the total magnetization and susceptibility.

In order to study the effect of different exchange coupling interactions $J_{Ni\text{-}Ni}$, $J_{Cr\text{-}Cr}$ and $J_{Ni\text{-}Cr}$ on the behavior of the total magnetizations of the (HHA) NiCrGa, we illustrate in Figs. 6(a), 6(b) and 6(c) the obtained results for H = 1, T = 20 K and different crystal field values. In fact, Fig. 6(a) corresponds to the effect of the exchange coupling interaction $J_{Ni\text{-}Ni}$ for fixed values of Jcr-cr = $J_{Ni\text{-}Cr}$ = 1. From this figure, it is seen that the effect of increasing exchange coupling interaction $J_{Ni\text{-}Ni}$ is to reach the saturation values of the total magnetizations. Indeed, this saturation is positive for positive values of the crystal field Δ = +5 and 0, while this saturation is negative for Δ = -5. Also, for negative values of the parameter $J_{Ni\text{-}Ni}$, the total magnetizations are not affected by the increasing this parameter. In Fig. 6(b), we provided the effect of varying the exchange coupling interaction parameter $J_{Cr\text{-}Cr}$ on the behavior of the total magnetizations. From this figure, it is clear that for negative values of the parameter $J_{Ni\text{-}Cr}$, the total magnetizations are not affected neither by the increasing effect of $J_{Ni\text{-}Cr}$, for its negative values, nor by the variations of the crystal field Δ, see Fig. 6(b). For positive values of the parameter $J_{Cr\text{-}Cr}$, the saturation of the total magnetizations is positive for positive values of the crystal field Δ = +5 and 0, whereas for Δ = -5, the saturation is negative. Contrary to Fig. 6(a), Fig. 6(c) shows a similar, but inverse, behavior in the sign of the total magnetization. The only difference is that for Δ = 0, the total magnetization undergoes a similar behavior to that one of the value Δ = -5. These figures show that the transitions of the magnetizations are of second-order type.

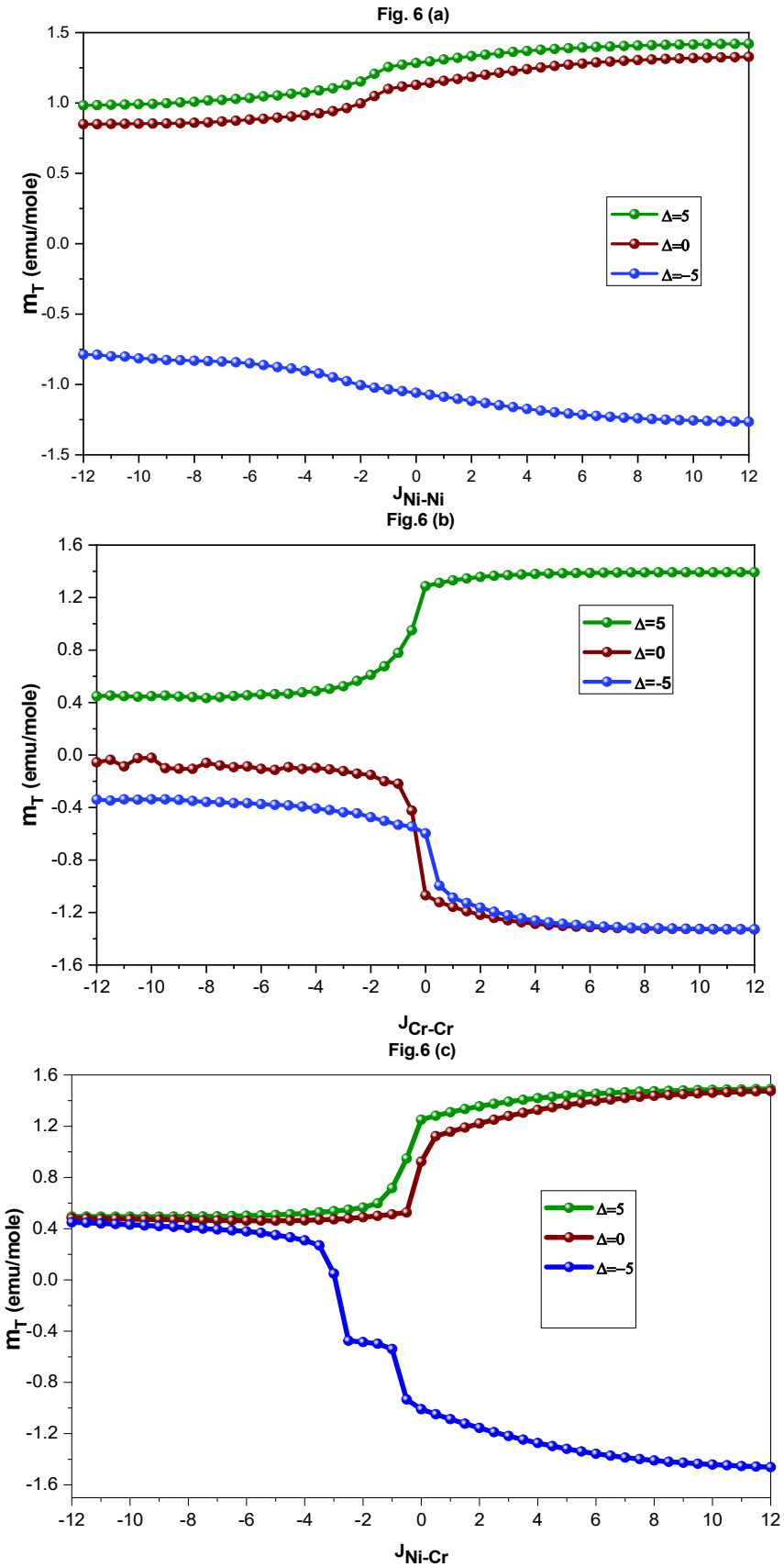

FIG. 6. The total magnetization of the half-Heusler alloy NiCrGa for H = 1, T = 20 K and selected values of the crystal field: Δ = -5, 0 and +5: (a) as a function of the exchange coupling interaction J_{Ni-Ni} for $J_{Cr-Cr} = J_{Ni-Cr} = 1$, (b) as a function of the exchange coupling interaction J_{Cr-Cr} for $J_{Ni-Ni} = J_{Ni-Cr} = 1$ and (c) as a function of the exchange coupling interaction J_{Ni-Cr} for $J_{Ni-Ni} = J_{Cr-Cr} = 1$.

To complete this study, we provide Figs. 7(a), 7(b) and 7(c) that show the hysteresis loops of the (HHA) NiCrGa, as a function of the external magnetic field H. In Fig. 7(a), we illustrate the obtained results for T = 15, Δ = 0 and selected different values of the exchange couplings. This figure shows that, when all exchange coupling interactions take the value +1, the surface of the hysteresis cycle is maximum. When fixing the value -1 of $J_{Cr\text{-}Cr}$, the surface of the cycle decreases and the steps corresponding to intermediate states are appearing. For $J_{Ni\text{-}Cr}$ = -1, the surface of the cycle decreases more and more. This surface tends towards the null value when imposing the value -1 for all exchange coupling interactions.

In order to show the effect of varying the temperature on the hysteresis cycles, we plot in Fig. 7(b) such behavior for Δ = 1, $J_{Ni\text{-}Ni}$ = $J_{Cr\text{-}Cr}$ = $J_{Ni\text{-}Cr}$ = 1 and selected different values of temperature T = 20 K, T = 55 K and T = 150 K. It is found that the surface of the hysteresis cycles decreases and consequently the corresponding coercive field, see Fig. 7(b). The effect of varying the crystal field on the hysteresis loops is summarized in Fig. 7(c) for T = 25 K, $J_{Ni\text{-}Ni}$ = $J_{Cr\text{-}Cr}$ = $J_{Ni\text{-}Cr}$ = 1 and selected values of the crystal field Δ = 0, Δ = 2 and Δ = 4. It is clear that when increasing the crystal field, the surface of the loops increases and *vice versa*. To confirm such results, we illustrate in Fig. 8 the coercive field dependency on the crystal field for T = 25 K and $J_{Ni\text{-}Ni}$ = $J_{Cr\text{-}Cr}$ = $J_{Ni\text{-}Cr}$ = 1. It is found that when increasing the crystal field, the corresponding coercive field increases to reach the value H_c = 3.75 at the crystal field value of Δ = 4.

Fig.7 (a)

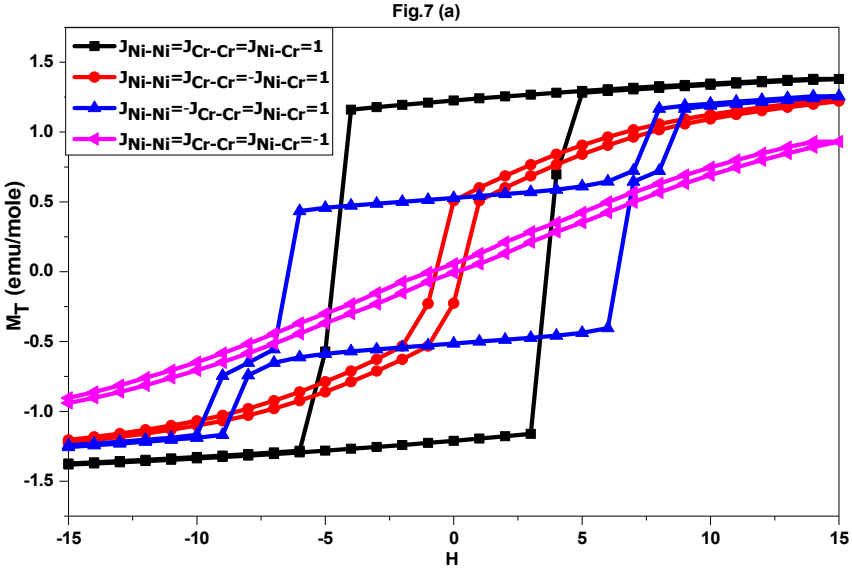

Fig. 7 (b)

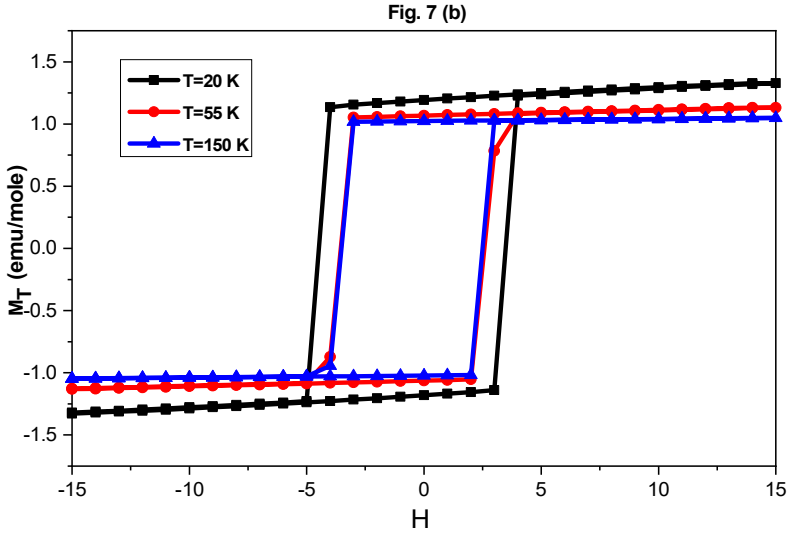

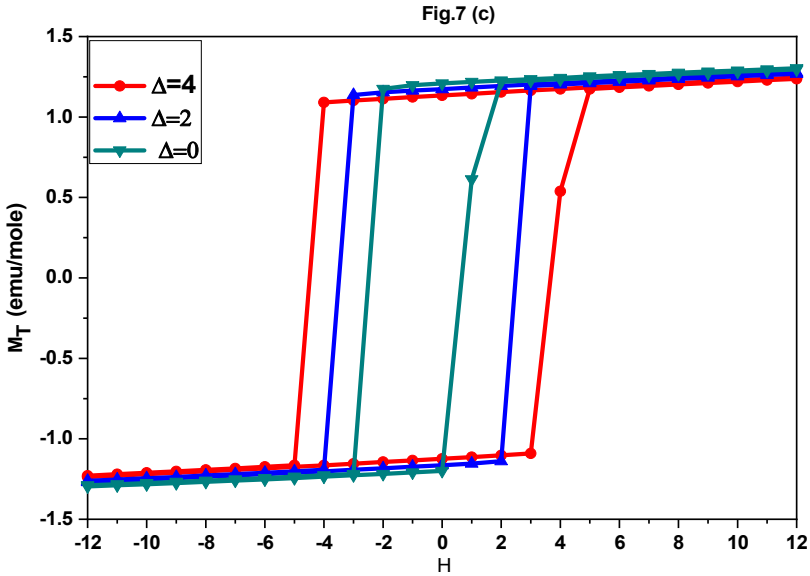

FIG. 7. Hysteresis loops of the half-Heusler alloy NiCrGa: (a) for T = 15 K, Δ = 0 and selected different values of the exchange coupling, (b) for Δ = 1, $J_{Ni-Ni} = J_{Cr-Cr} = J_{Ni-Cr} = 1$ and selected different values of temperature T = 20 K, T = 55 K and T = 150 K and (c) for T = 25 K, $J_{Ni-Ni} = J_{Cr-Cr} = J_{Ni-Cr} = 1$ and selected values of the crystal field Δ = 0, Δ = 2 and Δ = 4.

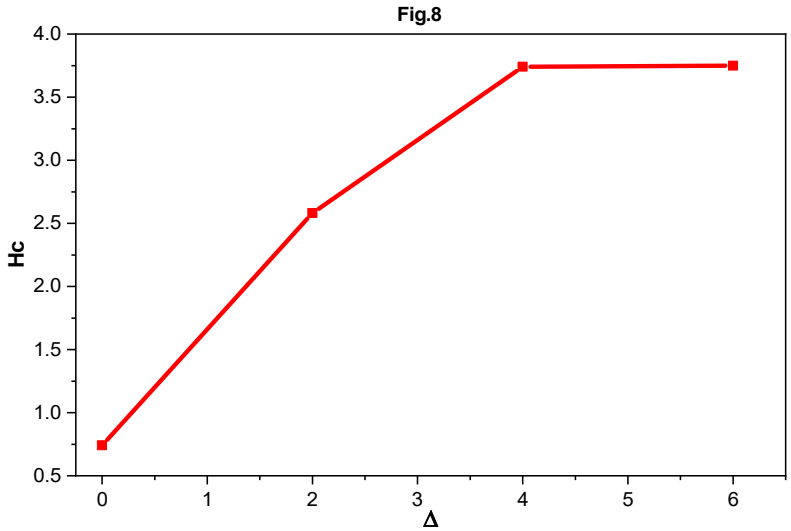

FIG. 8. Coercive field of Heusler alloy NiCrGa dependency on the crystal field for T = 25 K and $J_{Ni-Ni} = J_{Cr-Cr} = J_{Ni-Cr} = 1$.

5. Conclusion

In this paper, we have studied the electronic and magnetic properties as well as the critical behavior of the NiCrGa alloy using Monte Carlo simulations and DFT calculations.

The density of states (DOS) showed that this material exhibits a nearly half-metallic (HM) behavior. Moreover, the SP rule has been confirmed when using the magnetic moments of the individual constituents of the NiCrGa compound.

On other hand, the Monte Carlo method has been performed under the Metropolis algorithm to simulate the critical behavior of the half-Heusler NiCrGa alloy. Also, we have presented and discussed the magnetizations and susceptibilities as functions of temperature and other physical parameters.

To complete this study, we presented and illustrated the hysteresis loops of the (HHA) NiCrGa, for selected values of temperature, exchange coupling interactions and crystal field. It is found that when increasing the crystal field, the surface of the loops increases and *vice versa*. In particular, we have shown that when increasing the crystal field, the corresponding coercive field increases.

References

[1] Prinz, G.A., Phys. Today, 48 (1995) 58.

[2] Kobayashi, K.I., Kimura, T., Sawada, H., Terakura, K. and Tokura, K., Nature, 395 (1998) 677.

[3] Park, J.H., Vescovo, E., Kim, H.J., Kwon, C., Ramecsh, R. and Venkatesan, T., Nature, 392 (1998) 794.

[4] Hashemifar, S.J., Kratzer, P. and Scheffler, M., Phys. Rev. Lett., 94 (2005) 096402.

[5] Idrissi, S., Labrim, H., Ziti, S. and Bahmad, L., Journal of Superconductivity and Novel Magnetism, 33 (2020) 3087.

[6] Idrissi, S., Labrim, H. and Ziti, S., Appl. Phys. A, 126, (2020) 190.

[7] Idrissi, S., Labrim, H., Ziti, S. and Bahmad, L., Physics Letters A, 384 (24) (2020) 126453.

[8] Idrissi, S., Bahmad, L., Khalladi, R., El Housni, I., El Mekkaoui, N., Mtougui, S., Labrim, H. and Ziti, S., Chinese Journal of Physics, 60 (2019) 549.

[9] Zhang, L., Wang, X. and Cheng, Z., J. Alloys Compd., 718, (2017) 63.

[10] Gao, G.Y., Hu, L., Yao, K.L., Luo, B. and Liu, N., J. Alloys Compd., 551 (2013) 539.

[11] de Groot, R.A., Mueller, F.M., van Engen, P.G. and Buschow, K.H.J., Phys. Rev. Lett., 50 (1983) 2024.

[12] Kulatov, E. and Mazin, I.I., J. Phys.: Condens. Matter, 2 (1990) 343.

[13] Ebert, H. and Schutz, G., J. Appl. Phys., 69 (1991) 4627.

[14] Wang, X., Antropov, V.P. and Harmon, B.N., IEEE Trans. Magn., 30 (1994) 4458.

[15] Youn, S.J. and Min, B.I., Phys. Rev. B, 51 (1995) 10436.

[16] Otto, M.J., van Woerden, R.A.M., van der Valk, P.J., Wijngaard, J., van Bruggen, C.F. and Haas, C., J. Phys.: Condens. Matter, 1 (1989) 2341.

[17] Helmholdt, R.B., de Groot, R.A., Muller, F.M., van Engen, P.G. and Buschow, K.H.J., J. Magn. Magn. Mater., 43 (1984) 249.

[18] Kabani, R., Terada, M., Roshko, A. and Moodera, J.S., J. Appl. Phys., 67 (1990) 4898.

[19] Tanaka, C.T., Nowak, J. and Moodera, J.S., J. Appl. Phys., 81 (1997) 5515.

[20] Hordequin, C., Nozieres, J.P. and Pierre, J., J. Magn. Magn. Mater., 183 (1998) 225.

[21] Caballero, J.A., Park, Y.D., Childress, J.R., Bass, J., Chiang, W.-C., Reilly, A.C., Pratt, W.P. and PetroffFero, J.A., J. Vac. Sci. Technol. A, 16 (1998) 1801.

[22] Moradi, M., Taheri, N. and Rostami, M., Phys. Lett. A, 382 (41) (2018) 3004.

[23] Damewood, L., Busemeyer, B., Shaughnessy, M., Fong, C.Y., Yang, L.H. and Felser, C., Phys. Rev. B, 91 (2015) 064409.

[24] Umamaheswari, R., Yogeswari, M. and Kalpana, G., J. Magn. Magn. Mater., 350 (2014) 167.

[25] Dehghan, A. and Davatolhagh, S., J. Alloys Compd., 772 (2019) 132.

[26] Montag, B.W., Reichenberger, M.A., Arpin, K.R., Sunder, M., Nelson, K.A., Ugorowski, P.B. and McGregor, D.S., J. Cryst. Growth, 412 (15) (2015) 103.

[27] Zhang, R.L., Damewood, L., Fong, C.Y., Yang, L.H., Peng, R.W. and Felser, C., AIP Adv., 6 (2016) 115209.

[28] Luo, H., Zhu, Z., Liu, G., Xu, S., Wu, G., Liu, H., Qu, J. and Li, Y., Physica B: Condensed Matter, 403 (1) (2008) 200.

[29] Harmening, T., Eckert, H. and Pöttgen, R., Solid State Sci., 11 (2009) 900.

[30] Roy, A., Bennett, J.W., Rabe, K.M. and Vanderbilt, D., Phys. Rev. Lett., 109 (2012) 037602.

[31] Chadov, S., Qi, X., Kübler, J., Fecher, G.H., Felser, C. and Zhang, S.C., Nat. Matters, 9 (2010) 541.

[32] Amudhavalli, A., Rajeswarapalanichamy, R. and Iyakutti, K., Computational Materials Science, 148 (2018) 87.

[33] Baral, M., Chattopadhyay, M.K., Jangir, R., Chakrabarti, A. and Ganguli, T., Journal of Magnetism and Magnetic Materials, 475 (2019) 675.

[34] Idrissi, S., Ziti, S., Labrim, H. and Bahmad, L., Materials Science in Semiconductor Processing, 122 (2021) 105484.

[35] Idrissi, S., Ziti, S., Labrim, H. and Bahmad, L., Journal of Materials Engineering and Performance, 29 (11) (2020) 7361.

[36] Giannouzzi, P. *et al*., J. Phys.: Condens. Matter, 21 (2009) 395502.

[37] Vanderbilt, D., Phys. Rev. B, 41 (1990), 7892.

[38] Perdew, J.P., Burke, K. and Ernzerhof, M., Phys. Rev. Lett., 77 (1996) 3865.

[39] Perdew, J.P., Chevary, J.A., Vosko, S.H., Jackson, K.A., Pederson, M.R., Singh, D.J. and Fiolhais, C., Phys. Rev. B, 46 (1992) 6671.

[40] Momma, K. and Izumi, F., J. Appl. Crystallogr., 44 (2011) 1272.

[41] Özdoğan, K., Şaşıoğlu, E. and Galanakis, I., Journal of Applied Physics, 113 (19) (2013) 193903.

[42] Skaftouros, S., Ozdoğan, K., Şaşıoglu, E. and Galanakis, I., Phys. Rev. B., 87 (2013) 024420.

[43] Boumia, L., Dahmane, F., Doumi, B., Rai, D.P., Shakeel, A., Khandy, H., Khachai H. and Meradji, A.H., Chinese. J. Phys., 59 (2019) 281.